Chemical Geology 339 (2013) 30–42

Contents lists available at SciVerse ScienceDirect

Chemical Geology

journal homepage: www.elsevier.com/locate/chemgeo

Gas chemistry and nitrogen isotope compositions of cold mantle gases from Rungwe Volcanic Province, southern Tanzania

J.M. de Moor [a,*], T.P. Fischer [a], Z.D. Sharp [a], D.R. Hilton [b], P.H. Barry [b], F. Mangasini [c], C. Ramirez [d]

[a] Department of Earth and Planetary Sciences, MSC 03 2040, 1 University of New Mexico, Albuquerque, NM 87131-0001, USA
[b] Fluids and Volatiles Laboratory, Scripps Institution of Oceanography, UCSD, La Jolla, CA 92093-0244, USA
[c] Department of Mining and Mineral Processing Engineering, University of Dar Es Salaam, PO Box 35131, Dar Es Salaam, Tanzania
[d] Centro de Investigaciones en Ciencias Geologicas, Escuela Centroamericana de Geologia, Universidad de Costa Rica, San José, Costa Rica

ARTICLE INFO

Article history:
Accepted 9 August 2012
Available online 17 August 2012

Keywords:
East African Rift
Gas geochemistry
Nitrogen isotope method
Nitrogen isotopes
Mantle degassing
Geothermal

ABSTRACT

We report the first complete bulk gas chemistry and nitrogen isotope data for geothermal volatiles from the Rungwe Volcanic Province, located in the western branch of the East African Rift north of Lake Malawi. Temperatures of springs and gas emissions at Rungwe vary from 13 °C to 65 °C with the highest temperatures observed at the springs in the northern and southern lowlands. The vigorously degassing cold CO_2 vents and springs have temperatures between 13 °C and 36 °C and are located at higher elevation than the hot springs. The gas compositions are ~99% CO_2, 0.0008 to 0.0078 mmol/mol H_2, 0.0004 to 0.062 mmol/mol He, 0.08 to 0.77 mmol/mol Ar, 3.1 to 28.5 mmol/mol N_2, 0.4 to 3.73 mmol/mol O_2, <0.002 to 1.541 mmol/mol CH_4, <0.001 to 0.009 mmol/mol CO, and are poor in H_2S (0.045 to 0.201 mmol/mol). The CO_2 flux at a local gas collection plant is estimated to be 1.6×10^5 mol/year. Gas geothermometry indicates a range of equilibration temperatures from >250 °C (from CO_2–Ar) to ~60 °C (from H_2–Ar), which is interpreted to reflect deep equilibration with hot saline fluids and shallow re-equilibration of kinetically fast gas geothermometers with cold meteoric recharge from the highlands. N_2–He–Ar systematics show that the gases fall on a well-defined mixing line between upper mantle or sub-continental lithospheric mantle and air saturated water endmembers. Details of an improved method for analyzing nitrogen isotope compositions in gas samples are presented. Nitrogen isotope compositions ($\delta^{15}N$ values) range between +2‰ and −5.9‰, overlapping with the upper mantle range, with only one sample location displaying $\delta^{15}N$ values greater than air (0‰). The results emphasize the importance of the East African Rift as a potential, but poorly constrained, contributor of sub-continental lithospheric mantle volatiles to the Earth's surface even in regions that are currently volcanically dormant, but are seismically active.

1. Introduction

Rungwe Volcanic Province (RVP) is located in southern Tanzania on the western branch of the East African Rift (EAR) system and represents the southernmost expression of rift-related volcanism (Fig. 1, inset). Volcanism, topographic uplift, and extension along the 2000 km long EAR are manifestations of deep mantle upwelling associated with the African Superplume, which is a tilted low-velocity zone that impinges on the base of the African continent beneath East Africa and may originate at the core–mantle boundary beneath southern Africa (Nyblade and Robinson, 1994; Ritsema et al., 1999). The strongest geochemical evidence for lower mantle contribution to EAR volcanism comes from helium isotope compositions of volcanic rocks. Oligocene to Holocene lavas from Ethiopia indicate a significant lower mantle contribution (Marty et al., 1996; Scarsi and Craig, 1996; Pik et al., 2006). Recently, Hilton et al. (2011) reported lower mantle signatures (elevated $^3He/^4He$ compositions up to 15 R_A where R_A refers to the He isotope composition of the sample relative to the $_3He/_4He$ ratio of air) in some RVP scoria and lavas, suggesting that upwelling lower mantle drives volcanism along the entire EAR.

Carbon-rich volcanic emissions are common in Africa, yet studies of gas geochemistry are sparse. The famous catastrophic gas eruptions from Lakes Monoun and Nyos in Cameroon killed 37 and 1700 people in 1984 and 1986, respectively, due to magmatic CO_2 gas accumulation in the lakes followed by limnic overturn and degassing in response to depressurization (Kusakabe et al., 1989; Giggenbach, 1990). Diffuse CO_2-rich magmatic gas emissions in the Goma region (Democratic Republic of Congo) present a continuous lethal hazard to the local inhabitants (Vaselli et al., 2003; Smets et al., 2010; Tedesco et al., 2010), and accumulation of associated CO_2 and CH_4 in Lake Kivu (Tassi et al., 2009) presents a potentially catastrophic hazard similar to those at Lakes Nyos and Monoun. Anecdotal evidence collected in the field

* Corresponding author.
E-mail address: mdemoor@unm.edu (J.M. de Moor).

0009-2541/$ – see front matter © 2012 Elsevier B.V. All rights reserved.
http://dx.doi.org/10.1016/j.chemgeo.2012.08.004

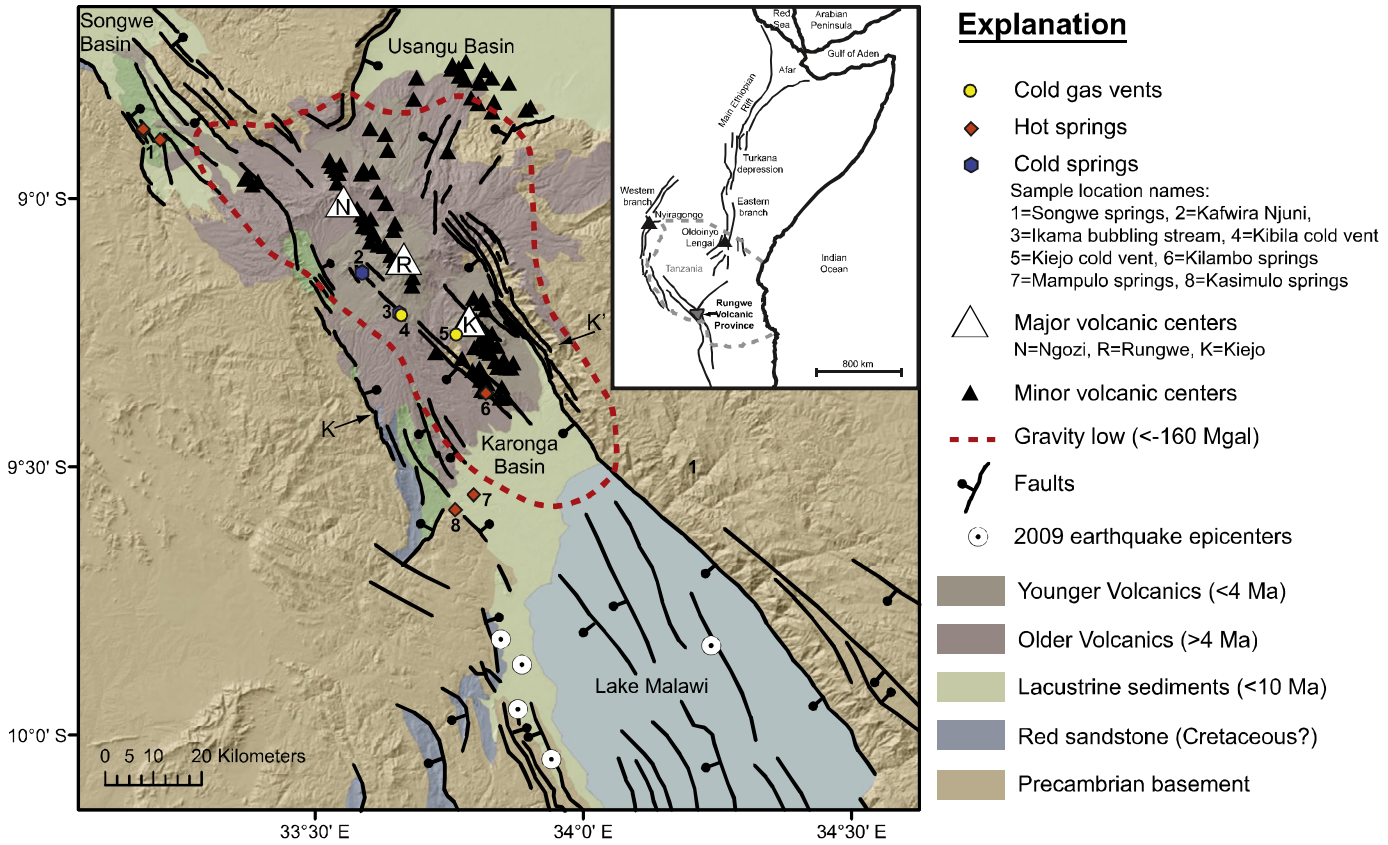

Fig. 1. Map of the RVP with sample locations. Inset is a schematic map of the East African Rift system showing major regional structures, the location of the RVP in the western branch of the rift of southern Tanzania, and major active volcanoes discussed in the text. The main map shows generalized geology and structure after Harkin (1960) and Ebinger et al. (1989) over shaded topography, volcanic centers, and epicenter locations of the 2009 Karonga earthquakes from Biggs et al. (2010). The area enclosed by the dashed red line is a gravity low (<−160 MGal), which was interpreted by Ebinger et al. (1989) to reflect low density magma intrusions at depth. Volcanoes and geothermal features generally coincide with the gravity low, and are aligned on major extensional faults. Arrows mark the location of the K and K′ cross section shown in Fig. 11.

during our sampling campaign in the RVP area suggests that incidents of asphyxiation of people and animals due to CO_2 accumulation in low lying areas are relatively common, however a thorough analysis of the hazards associated with CO_2 degassing at RVP is needed.

Volatile fluxes from continental rifts and the EAR are not well characterized, except for gas fluxes from persistently degassing volcanoes in the region. Volatile emissions from Nyiragongo present some of the most significant volcanic SO_2 and CO_2 contributions to the atmosphere (~30 kg/s SO_2 and ~100 kg/s CO_2; Sawyer et al., 2008). Oldoinyo Lengai Volcano in northern Tanzania is one of the largest sources of volcanogenic CO_2 in the world (Koepenick et al., 1996) and is the only active carbonatite volcano on Earth. Fischer et al. (2009) and de Moor et al. (submitted for publication) show that the volatile and trace element compositions of CO_2-rich magmatic products from Oldoinyo Lengai are consistent with a MORB-like mantle source that is not unusually volatile-rich. Observations of extensive volatile degassing in a rift setting provide important constraints on the nature of the sublithospheric mantle and the efficiency of mass transfer from the mantle to the atmosphere over a wide region. Here, we report the first total gas and nitrogen isotope compositions of gas emissions from fault-controlled cold CO_2 vents and bubbling springs of the RVP in order to determine source characteristics and processes involved in volatile transfer from mantle and crustal regions to surface reservoirs.

2. Background

2.1. Local geology

The RVP covers an area of ~1500 km^2 and occurs at the junction of three half-graben basins (Karonga, Songwe, and Usangu basins; Fig. 1). Rifting and volcanism at RVP began in the mid-Miocene (Ebinger et al., 1989) and the most recent volcanic eruption occurred in ~1800 at Kiejo Volcano (Fig. 1; Harkin, 1960). The uplifted highlands adjacent to the basins are composed of pre-Cambrian to Tertiary metamorphic, intrusive and sedimentary rocks. The recent basin fill includes lacustrine sediments from an ancestral Lake Malawi and alluvial fans shed from the highland rift flanks.

Volcanic products range from highly silica-undersaturated mafic lavas to trachytic and phonolitic Plinian deposits (Harkin, 1960; Furman, 1995; Fontijn et al., 2010). Three main volcanic centers dominate recent volcanism: Ngozi caldera, which last erupted <1 ka before present (Plinian trachytic); Rungwe Volcano, which last erupted <1.5 ka before present (explosive phonolitic); and Kiejo Volcano, which last erupted basaltic lava and scoria in ~1800 (Ebinger et al., 1989; Fontijn et al., 2010). Monogenetic volcanic centers are common in RVP, including maar craters, which are indicative of phreatic eruptions due to interaction between basaltic magmas and a shallow aquifer (Delalande et al., 2008). The location of the major and minor volcanic centers is strongly controlled by normal and transfer faults (Fig. 1; Ebinger et al., 1989; Fontijn et al., 2010), and is also correlated with a Bouger gravity low (Fig. 1) that was interpreted by Ebinger et al. (1989) to correspond to low density magmatic material at shallow crustal levels. Extensional faults at RVP are dominantly oriented NW–SE, with an additional subset oriented ENE–WSW (Fontijn et al., 2010). Ebinger et al. (1989) suggested that volcanism at RVP preferentially occurs at the propagating tips of border and transfer faults.

The RVP area is seismically active as evidenced by the December 2009 Karonga earthquakes, which had Mw > 5.5 (Biggs et al., 2010) and caused the deaths of 5 local inhabitants. A magnitude 7.4 earthquake occurred in the Rukwa Rift (north of the Songwe basin) in 1910

(Ambraseys, 1991). Camelbeeck and Iranga (1996) reported earthquake epicenters for 200 earthquakes recorded between Lake Tanganyika and Lake Malawi between 1992 and 1994. These events show that faults in the Songwe and Karonga basins are active while the Usangu basin faults are aseismic.

2.2. The hydrothermal system

Fig. 1 shows the locations of hydrothermal features in the area sampled for this study. The distribution of springs is associated with fault locations. The Songwe bubbling springs in the north are located on the NW trending border fault on the western margin of the Songwe basin, the springs and gases of the central Karonga basin are located on the faults associated with the NW trending Mbaka transfer fault system, and the Kasimulo and Mampulo springs are located at intersections between NNW trending faults and a major ENE trending structure. Numerous maar crater lakes are found in the area, especially along the Mbaka fault (Fig. 1) and the salinity of these lakes increases with proximity to faults, suggesting hydrothermal fluid input (Delalande et al., 2008). The Ngozi caldera hosts a large (2.5 km × 1.5 km × 75 m deep) crater later. The location of these lakes on faults, which also provide conduits for volatiles, in a seismically active area raises the possibility of CO_2 accumulation in deep lake waters and, consequently, of limnic eruptions (e.g. Giggenbach, 1990). This potential hazard is in need of further assessment.

Temperatures of springs and gas emissions vary from 13 °C to 65 °C with the highest temperatures observed in the low-lying areas to the north and south of the central volcanic highlands (Fig. 1). The central zone springs and CO_2 vents close to the volcanic highlands recharge zone (Delalande et al., 2011) have lower temperatures between 13 °C and 36 °C. Local annual rainfall in the highlands is ~2 m/year. A CO_2 collection plant, located on the slopes of Kiejo Volcano, compresses gas collected directly from shallow (~60 m) boreholes. The plant has been operational since 1982 and the compressed gas is used by the carbonated beverage industry.

Pik et al. (2006) reported $^3He/^4He$ ratios from Rungwe geothermal fluids, and showed that helium isotope systematics indicate contribution from MORB-like fluids with measured $^3He/^4He$ compositions up to 7.8 R_A. Notably, new $^3He/^4He$ data from phenocrysts indicate a lower mantle helium contribution with values up to 15 R_A (Hilton et al., 2011). Delalande et al. (2011) studied the chemistry and isotopic compositions of water from the Rungwe region, and concluded that the chemistries are consistent with mixing between deep hot saline waters (electric conductivity 5000 to 10,000 μS cm^{-1}, Na-HCO_3(Cl) type, pH 7.0 to 7.9; Delalande et al., 2011) and cold meteoric water. According to water chemistry geothermometers (Na–K–Mg geothermometer of Giggenbach (1988)), the deep hot saline fluids originate from a hydrothermal reservoir at >110 °C (up to 185 °C), and the cold meteoric water is derived from recharge at high elevation from the surrounding mountains and large volcanoes (Delalande et al., 2011). Interestingly, the focus of magmatic activity and edifice building around the intersection of the three basins results in lower temperature hydrothermal features due to higher rainfall and colder recharge, whereas the hottest surface hydrothermal features are located on the periphery of the magmatic focus. Delalande et al. (2011) report $\delta^{13}C$ for CO_2 gas and dissolved inorganic carbon between −20‰ and −2‰, which they interpreted to reflect contributions from magmatic CO_2 (with calculated source $\delta^{13}C$ composition between −4.9‰ and −8.6‰) as well as from isotopically light biogenic carbon.

3. Sampling and analytical methods

Gas samples were collected using evacuated Giggenbach bottles containing ~50 ml of 4 N NaOH solution using standard techniques described by Giggenbach and Goguel (1989). Two sample types were collected: 1. gas samples from bubbling springs and CO_2 vents, and 2. water samples from springs that were not actively bubbling. Gas samples from bubbling springs were collected by placing an inverted funnel over the bubbling area in the bottom of the spring, with the funnel connected to silicon tubing and the Giggenbach bottle. The funnel was held as close to the bubbling outlet on the floor of the springs as possible, and remained completely submerged during sampling to minimize sampling-related air contamination. Gas samples from vents were collected by inserting a titanium tube into the orifice or burying a funnel over the excavated vent, with the funnel or tube connected to the Giggenbach bottle with silicon tubing. In both cases, gas was slowly allowed to pass into the Giggenbach bottle, after thoroughly flushing the sampling system, and acid gases are absorbed by the NaOH solution while the low solubility and inert gases fill the headspace. In the case of water samples, a tube was inserted as deep as possible into the outflow area, gas-rich water was then pulled (siphoned) through the silicon tubing, which was in series with the Giggenbach bottle. The vacuum in the Giggenbach bottle pulls the gas-rich hydrothermal water into the sample bottle and low solubility/inert gases dissolved in the water partition into the headspace while acid species remain in solution due to the presence of NaOH solution in the bottle. Our samples are complemented by the data of Barry et al. (2013–this issue) who sampled for He and C in series with our sampling set-up.

Headspace gases were analyzed on a Gow-Mac Series 600 gas chromatograph and on a Pfeiffer Quadrupole Mass Spectrometer at the University of New Mexico. For the gas chromatography (GC) measurements, gas separation was accomplished using a Hayes Sep precolumn and 5 Å molecular sieve columns. Argon, N_2, He, H_2, and O_2 were analyzed on a thermal conductivity detector and CO and CH_4 were analyzed on a flame ionization detector after conversion of CO to CH_4 by a methanizer, following the method of Giggenbach and Goguel (1989). The analytical uncertainty of the GC measurements is estimated at ± 5%. The presence of oxygen may be problematic in GC analyses because a significant amount of O_2 in the sample interferes with the analysis of Ar (Zimmer et al., 2004; Elkins et al., 2006). Oxygen partial pressure is determined by separation via a 4 m 5 Å molecular sieve column utilizing Ar carrier gas. Argon partial pressure is determined via separation on a 1.5 m 5 Å molecular sieve column with H_2 carrier gas, followed by conversion of O_2 to H_2O by reaction with the carrier gas in a 0.5 m 5 Å molecular sieve column at 200 °C. However, at high O_2 concentration (above 4.5 wt.% in headspace gas; Elkins et al., 2006) incomplete O_2 combustion can result in erroneous Ar determination. To overcome this problem, the aliquots of headspace gas were analyzed for N_2/Ar and N_2/He on a Pfeiffer quadrupole mass spectrometer at the University of New Mexico (QMS; mass range from 0 to 120 amu) equipped with a Faraday detector and operated in dynamic mode. Calibration of the QMS was performed with appropriate calibration gases (Scott Specialty Gases; Mix 14: 1% Ar, 1% He, 1% O_2, 1% CH_4, 1% CO, 95% N_2; Mix 104: 99.995% Ar, 0.005% N_2) and data processing using the Quadstar software that allows for correction of potential mass interferences. The QMS analyses have a precision of <0.1% (concentration), except for He in samples with low partial pressures where the uncertainty is ± 1%. The measured partial pressure of each gas species (from GC analysis), the total pressure in the headspace, and the volume of the headspace were used to calculate the total moles of N_2, O_2, H_2, CH_4, and CO. Argon and He concentrations were calculated using the N_2 concentrations and the N_2/Ar and N_2/He (respectively) from QMS measurements. The total headspace pressures of all samples (average = 98 mbar) were much lower than atmospheric pressure suggesting that contamination due to leakage during sample transport was minimal.

Carbon dioxide concentrations were determined by titration using 0.1 N HCl. Chloride and total S concentrations were measured by ion chromatography on aliquots of caustic solution that were oxidized by addition of hydrogen peroxide (to convert all S to sulfate), diluted by a factor of ten, and filtered using Dionex OnGuard® II H cartridges to remove hydroxyl groups. Samples and a blank were analyzed on a Dionex ion chromatograph following the techniques of Mitchell et al. (2010). The concentrations measured in the blank were subtracted

from those measured in the sample. Sample concentrations were only slightly elevated above concentrations measured in the blank with the blank HCl concentrations about half of that measured in the sample (average) and sulfate concentration in the blank about 80% of that measured in the sample, indicating that HCl and total sulfur concentrations in the samples were barely above blank concentrations indicating that the gases are poor in S and HCl.

3.1. Determination of $\delta^{15}N$ values of gas samples

Nitrogen isotope analysis was conducted by an improved method on aliquots of headspace gas (prepared on a vacuum line) using a front-end valve switching assembly connected to a Finnigan GasBench and a MAT252 isotope ratio mass spectrometer at the University of New Mexico. Fig. 2 provides details of the method developed in our lab for the analysis of nitrogen isotope compositions in gas samples. The sealed glass tube containing the gas aliquot is scored and loaded into a tube breaker (Fig. 2a, *1*), which is flushed with ultra high purity helium gas at very high flow for 5 min. Blank analyses show that the N_2 background measured in the mass spectrometer after this flush step is extremely low with nitrogen peaks between 20 mV (equivalent to ~0.5 mbar headspace N_2) and 0 mV, (i.e. below detection limit, which is estimated to be ~10 mbar N_2 in sample headspace for $\delta^{15}N$ determination). Background levels are checked at the beginning and end of each analytical session. Once the cracker tube is flushed of any residual air, the six-way valve (Fig. 2a, *2*) of the injection system is switched to the load position (Fig. 2b, *2*), the glass sample tube is then broken, and the N_2 gas sample is carried by an ultra high purity helium stream through a NAFION water trap to the GasBench. It is imperative that both stainless steel vent tubes running off the eight-way valve at *3* in Fig. 2 are very long (>3 m) because when the sample is cracked the rapid drop in pressure in the tube cracker can result in back flushing through the vent, resulting in air contamination. Long vent tubes and therefore a large reservoir of ultra high purity He after the vent ports on the eight-way valve eliminate this problem because only He is introduced back into the sample loop. For extra caution and in order to monitor back flushing during analyses, we attach a wide diameter ~0.5 m long clear plastic tube to the exit of the vent tubes and submerge the end in water. Periodic switching of the eight-way valve injects 100 µl aliquots of the sample gas (Fig. 2a and b, *3*; fourteen aliquots per analysis) through a 30 m × 0.53 µm 5 Å molecular sieve (Chrompack Varian) column heated to 40 °C (Fig. 2a and b, *4*). The sample aliquots are then passed to the Finnigan MAT 252 mass spectrometer via an open split and analyzed in continuous flow mode. Fig. 3 shows typical sample N_2 peaks (sample from Kilambo springs, Fig. 1, $\delta^{15}N_{air}$ − 5.0‰) measured on the mass spectrometer with measured signal for masses 28, 29, and 30.

Known gas mixtures containing CO and CH_4 (Scott Specialty Gases; Mix 218: 1% CO_2, 1% CO, 1.03% O_2, 1% H_2, 0.993% CH_4, 94.977% N_2) are analyzed to ensure that these species are efficiently separated from N_2 because CO and hydrocarbon species can interfere with N_2 peaks and result in inaccurate $\delta^{15}N$ values. Fig. 3 shows the clear separation between a small peak from an unknown gas species and the succeeding large N_2 peaks in a typical gas sample. Additional aliquots of gas samples with problematic high CO or hydrocarbon concentrations can be prepared for re-analysis with ~0.5 g of cupric

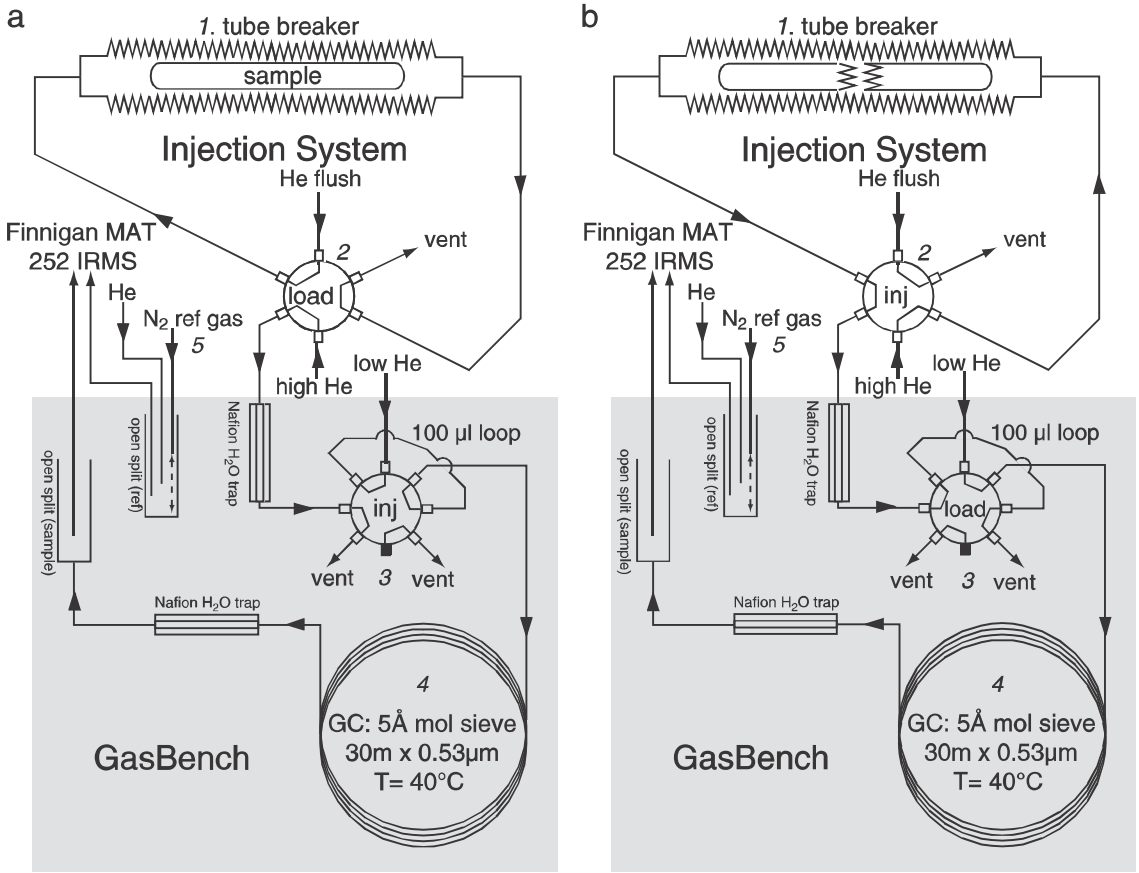

Fig. 2. Schematic diagram of the laboratory method used for introduction of gas samples into the isotope ratio mass spectrometer for nitrogen isotope analysis. Panel a shows the setup in load mode in which a high He flow purges the sample tube breaker to allow rapid flushing of the system after sample loading. Panel b shows the setup in injection mode after the sample tube is cracked. The gas sample is carried to the gas bench and 100 µl aliquots of the gas are injected into the IRMS via a chromatographic column and sample loop by the eight way valve switching between the load and inject positions. See text for details.

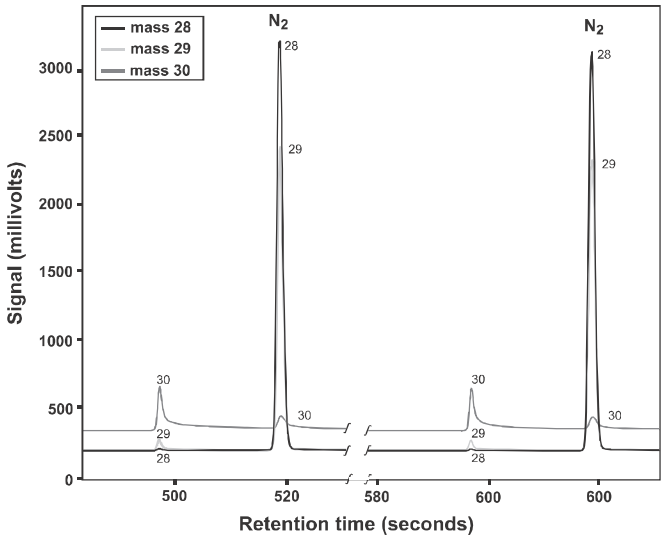

Fig. 3. Typical results of nitrogen isotope analysis of geothermal gas samples, showing signal voltages measured for masses 28, 29, and 30 versus retention time. The N_2 peaks are clearly separated from CO by the GC column and signal voltage decays rapidly to background levels after each sample injection. Each analysis (~15 min) consists of two injections of reference gas followed by 14 injections of sample gas and one injection of reference gas at the end.

oxide in the glass tubes and baked overnight in a furnace at 300 °C (higher temperatures result in deformation of the Pyrex glass sample tubes) to oxidize all C species to CO_2, which is adsorbed by the mol sieve GC column during analysis. The samples in this study did not display high CO or methane concentration and peak separation was efficient (Fig. 3), therefore no secondary preparation or re-analyses were necessary.

Each analytical run consists of two injections of reference gas (Fig. 2a and b, *5*) at the beginning of the sequence, followed by fourteen injections of sample gas (Fig. 3), and an injection of reference gas at the end of the sequence. Some samples were run multiple times, depending on the N_2 partial pressure in the glass sample tube. Air standards are prepared on the same vacuum line and with similar N_2 partial pressures to the samples. The standards are analyzed at the beginning, at the end, and after every five samples during analytical sessions. The measured $\delta^{15}N$ value for air varied by <0.2‰ (i.e. within analytical precision) during three consecutive days of analysis, and showed no dependence on N_2 partial pressure (i.e. peak amplitude) and no drift outside of analytical precision. The reported $\delta^{15}N$ sample values and analytical uncertainties are the mean and 1σ uncertainties, respectively, of between ten and sixteen measurements, normalized to the air standard. Typically, after cracking the sample and starting the analysis, the peak amplitudes rise rapidly from background after about 2–3 min and then decay slowly over time. Peaks with amplitudes between 10 V (saturation occurs at ~12 V) and 500 mV (using peaks below this voltage results in lower precision) on the mass 28 signal were used for calculating the mean $\delta^{15}N$ and the uncertainty of the analysis, and peaks from the rising signal portion of the analysis were ignored. The 1σ analytical precision is between ±0.1‰ and ±0.3‰, except for samples with low N_2 partial pressure (<~30 mbar in sample headspace), which have uncertainties of ±0.4‰ to ±0.5‰. This is an improvement over our previous method (Fischer et al., 2002; Zimmer et al., 2004) where analytical uncertainty was ±0.3‰ to ±0.6‰. Reruns of multiple sample aliquots were within analytical precision of one another. Fig. 4 shows the results of N isotope measurements performed on the Finnegan 252 stable isotope mass spectrometer where the majority of samples are clearly distinguishable from the air standards.

4. Results

Compositions of gas samples and gas + water samples are presented in Table 1. Gases are reported as dry (water-free) gas compositions. Nitrogen isotope compositions are reported in standard delta notation relative to air. All gases are extremely CO_2-rich, with most samples containing ~99% CO_2 (dry gas). The gases contain low concentrations of S (expressed as S_T, i.e. $H_2S + SO_2$) and HCl, with an average S/Cl of 9. The HCl in the gas samples is due to entrainment of small amounts of spring water or steam into the gas sample as is commonly observed during sampling of bubbling springs (e.g. Taran et al., 1998). Nitrogen is the second most abundant constituent after CO_2 in gas samples, accounting for between 3 and 28 mmol/mol. The gas samples contain between 0.4 and 3 mmol/mol O_2, whereas the gas + water phase samples contain up to 19 mmol/mol O_2. Argon contents vary between 0.08 and

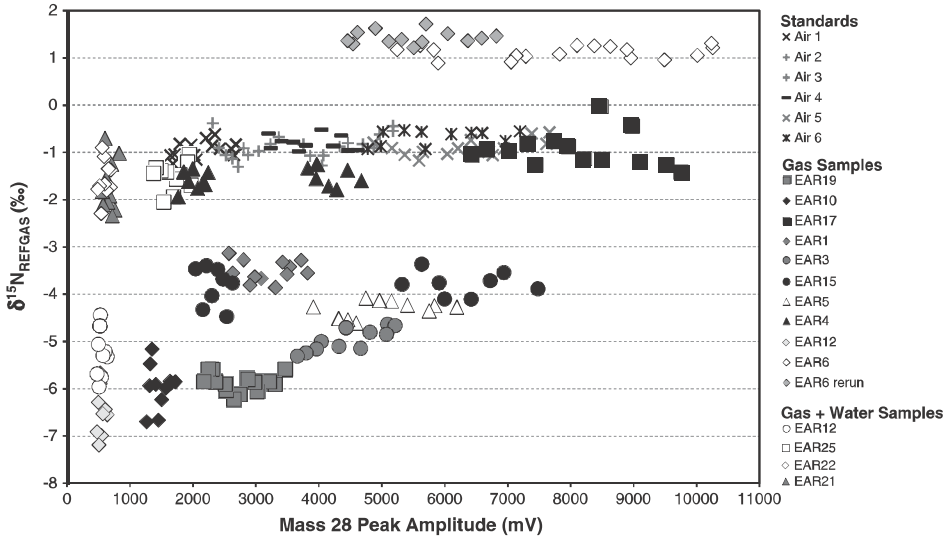

Fig. 4. Raw nitrogen isotope data plotted as $\delta^{15}N$ values measured relative to the composition of the internal reference gas versus amplitude of the mass 28 peak, which is proportional to nitrogen partial pressure. Air standards show no correlation with peak amplitude and do not vary outside of analytical precision. Precision of sample analyses is ±0.1‰ to ±0.3‰ for samples with peak amplitudes >1500 mV and is ±0.4‰ to ±0.5‰ for samples with peak amplitudes <1500 mV. With the exception of one sample, all of the RVP gases have $\delta^{15}N$ values lower than air.

Table 1
Compositions of gas (G) and hydrothermal fluid (F) samples from the RVP. "Fluid" refers to gas-rich water samples (with or without a free gas phase) from springs. Samples are listed according to location from north to south. Gas compositions are reported as mmol/mol dry gas. Hydrothermal fluid samples are reported as mmol/mol dissolved gas. Total sulfur (S_T) and HCl are not reported for hydrothermal fluid samples because SO_4^{2-} and Cl^- are present in the sampled hydrothermal water and analysis of the NaOH + liquid therefore gives misleading data irrelevant to the gas phase.

Sample location	Type	ID	T °C	Lat. °S	Long. °E	CO_2 mmol/mol	S_T mmol/mol	HCl mmol/mol	Ar mmol/mol	N_2 mmol/mol	He mmol/mol	H_2 mmol/mol	O_2 mmol/mol	CH_4 mmol/mol	CO mmol/mol	$\delta^{15}N_{Air}$ (‰)	σ
Songwe spring 2 overlook	F	EAR12	71	8.873	33.182	976	n.a.	n.a.	0.285	13.03	0.01929	0.0125	10.68	<dl	0.006	−5.9	0.5
Songwe spring 3 mesa	G	EAR1	64	8.875	33.182	994	0.128	0.007	0.133	4.46	0.00335	0.0021	1.63	0.014	0.001	−2.7	0.2
Songwe spring 1 quarry	G	EAR17	54	8.891	33.211	992	0.201	0.025	0.079	5.32	(0.00038)[a]	0.0027	2.67	0.002	0.002	−0.1	0.2
Kafwira Njuni/Place of Dead Birds	F	EAR25	20	9.139	33.589	954	n.a.	n.a.	0.978	25.27	(0.00014)[a]	0.0282	19.22	0.010	0.005	−0.6	0.2
Ikama Village bubbling stream	G	EAR6	23	9.213	33.655	968	0.047	0.017	0.771	28.46	0.00954	0.0008	2.77	<dl	<dl	2.0	0.1
Kibila cold vent	G	EAR5	13	9.217	33.659	991	0.079	0.005	0.164	6.01	0.02146	0.0036	2.34	0.250	<dl	−3.4	0.2
Kiejo cold vent	G	EAR3	15	9.253	33.763	990	0.098	0.009	0.178	6.69	0.01781	0.0015	2.97	0.093	0.009	−4.1	0.2
Kiejo cold vent	G	EAR10	15	9.253	33.763	996	0.072	0.005	0.079	3.12	0.02224	0.0039	0.99	0.121	0.004	−5.2	0.4
Kilambo springs	F	EAR2	57	9.364	33.818	986	n.a.	n.a.	0.180	10.64	<dl	0.0104	3.67	<dl	<dl	n.a.	n.a.
Kilambo springs	G	EAR19	36	9.364	33.818	988	0.045	0.044	0.203	7.66	0.00592	0.0038	3.73	0.026	0.002	−5.0	0.2
Mampulo spring 2	G	EAR4	55	9.552	33.796	991	0.157	0.019	0.162	6.53	0.06112	0.0057	0.40	1.500	<dl	−0.9	0.2
Mampulo spring 2	G	EAR15	55	9.552	33.796	987	0.115	0.027	0.213	8.36	0.06196	0.0078	2.20	1.541	<dl	−2.9	0.3
Mampulo spring 1	F	EAR13	60	9.552	33.798	990	n.a.	n.a.	nd	5.89	<dl	0.0060	2.23	1.657	<dl	n.a.	n.a.
Kasimulo spring	F	EAR21	52	9.583	33.762	988	n.a.	n.a.	0.134	7.52	0.00092	0.0054	4.68	0.011	<dl	−0.8	0.5
Kasimulo spring	F	EAR22	52	9.583	33.762	982	n.a.	n.a.	0.336	11.51	0.02463	0.0143	6.30	0.017	0.005	−0.6	0.4

[a] These samples had low total headspace pressure and these values are prone to substantial errors that may be within range of the detection limit.

2 mmol/mol in gas samples and reach up to 1 mmol/mol in gas + water phase samples. The helium contents of all samples range from below the detection limit of QMS measurements (~100 ppm; which equates to 0.0004 to 0.003 mmol/mol in terms of bulk composition for this dataset and is dependent on gas pressure in the sample headspace) to 0.06 mmol/mol. Hydrogen is present at low concentrations (0.0008 to 0.0277 mmol/mol) in all of the samples. Methane (<0.002 to 1.541 mmol/mol) contents are variable and typically higher than CO (<0.001 to 0.009 mmol/mol).

Fig. 5 shows that the samples from RVP are extremely CO_2-rich compared to samples from volcano-hosted geothermal systems (Goff et al., 2000 and references therein) and fall within the range of travertine-depositing springs from Italy (i.e. Chiodini, 1994) and those discharging along fault systems in the western USA (Crossey et al., 2009), consistent with extensive travertine deposits in the Rungwe region.

Fig. 6 shows a N_2–He–Ar ternary plot (Giggenbach, 1991) with compositions of RVP samples. Mantle-derived gases fall near the He apex of the plot because the accepted He/Ar and N_2/Ar ratios of the upper mantle are on the order of 1 (Burnard et al., 1997) and 80 (Marty and Zimmermann, 1999), respectively. Gases associated with arc volcanism typically have high N_2/He ratios due to N_2 addition to magma source regions from subducted sediments (e.g. Fischer et al., 1998). Air has a N_2/Ar ratio of 84, while air saturated water (ASW) has a N_2/Ar ratio of ~40 (temperature dependent). Most of the samples from RVP fall on a well-defined trend between the mantle endmember and air-saturated water, consistent with magmatic contribution as sampled at Oldoinyo Lengai (Fischer et al., 2009) and Lake Nyos (Giggenbach, 1990).

The nitrogen isotope ($\delta^{15}N_{Air}$) compositions of RVP samples vary between −5.2‰ and −0.1‰, except for one sample (EAR6 from Ikama Village bubbling spring) that has a positive value of +2.0‰. The nitrogen isotope composition of air is by definition 0‰. The nitrogen isotope composition of MORB varies from −2 to −8‰ (Marty and Zimmermann, 1999), while arc-related gases typically have positive $\delta^{15}N$ values (Sano et al., 2001; Fischer et al., 2002) due to addition of subducted slab derived sedimentary N_2, which usually has positive $\delta^{15}N$ values (~+7 ± 2‰; e.g. Peters et al., 1978; Sadofsky and Bebout, 2004; Li and Bebout, 2005), to the mantle wedge. The nitrogen isotope compositions of eclogitic and peridotitic diamonds typically display a wide range of values; however, the mean falls within the range of MORB (e.g. Cartigny, 2005). Similarly, the average nitrogen isotope composition of African diamonds falls within the range of MORB (e.g. Boyd et al., 1992; Cartigny, 2005; Palot et al., 2009). Fischer et al. (2009) reported a mean nitrogen isotope composition of −4.4‰ for three gas samples from Oldoinyo Lengai Volcano, located on the eastern branch of the EAR in northern Tanzania that have sub-continental lithospheric mantle (SCLM) or upper mantle-like noble gas isotope compositions and abundance ratios.

5. Discussion

5.1. Shallow processes

The RVP gas samples display N_2/Ar ratios that overlap with the MORB range, which is also within the range of air (80) to air saturated water (~40, temperature dependent). As can be seen from Fig. 6, samples with significant He contents (discussed in Sections 5.1 and 5.2), resulting in He/Ar > air (5×10^{-4}), are the most likely candidates of being the least contaminated by atmosphere-derived gases. These samples also have He/Ne ratios that are well in excess of air, consistent with a significant non-atmospheric helium input (Barry et al., 2013–this issue). Notably, our gas samples contain less than 0.3% O_2 and the majority of the water samples contain less than 1% O_2 (dry gas). Fig. 7 shows that samples plotting far from the air and air-saturated water endmembers, due to high He contents, have N_2/O_2 ratios that lie between those of air (3.7) and air-saturated water (temperature

dependent with N_2/O_2 decreasing with increasing temperature: 1.9 at 25 °C; 1.6 at 100 °C). This is consistent with the fact that the helium content of the atmosphere is low (5 ppm) and helium provides the strongest signal of mantle volatile degassing compared to other noble gases. Likewise CO_2/O_2 ratios of the gas discharges (~50 to ~1000) are several orders of magnitude higher than that of air (0.002). Nitrogen, on the other hand, is the most abundant gas in air (78%) and therefore air contamination can have a significant effect on the N_2/He ratios and nitrogen isotope composition of gas discharges. Despite the high concentration of nitrogen in air, pristine mantle gases discharge in all tectonic settings and samples from different types of gas emissions (fumaroles, geothermal wells and bubbling springs) show $\delta^{15}N$ signatures that deviate significantly from air (0‰) to both positive and negative values (Fischer et al., 1998; Sano et al., 2001; Fischer et al., 2002; Snyder et al., 2003; Elkins et al., 2006; Fischer et al., 2009; Inguaggiato et al., 2009).

Fig. 8 shows that a number of samples and particularly those from the cold gas vents, plot close to the upper mantle $\delta^{15}N$ endmember of -5 ± 3‰ of Marty and Zimmermann (1999) and have N_2/He ratios <1000. Four samples (one from Ikama Village, two from Mampulo spring, and one water sample from Kasimulo spring) are shifted towards the sediment endmember and lie on or below the mixing line between mantle and sediment. Three samples out of 13 in Fig. 8 lie close to the air endmember with both high ($>1\times10^4$) N_2/He ratios and $\delta^{15}N$ values near 0‰, consistent with a predominantly atmospheric source for N_2. These are Kasimulo spring duplicate (EAR21), Songwe spring1 (EAR17) and Kafwira Njuni (EAR25).

It is noteworthy that a significant number of samples fall outside of the polygon defined by simple mixing between the endmembers shown in Fig. 8. Three samples that best exemplify this observation are EAR1 (gas) and EAR12 (fluid) from Songwe springs ("SO" in Fig. 8) and EAR19 (gas) from Kilambo springs ("KI" in Fig. 8). These samples have negative nitrogen isotope compositions overlapping with the mantle range, but N_2/He ratios up to an order of magnitude higher than that of typical upper mantle (Marty and Zimmermann, 1999). The compositions of these samples require either an additional N_2 source with high N_2/He ($\geq$1000) and negative $\delta^{15}N$ composition (≤ -5.5‰), or a process by which N_2 and He experience elemental fractionation with or without associated isotopic fractionation. Nitrogen gas and He have similar solubilities in water and therefore a pure solubility/phase separation

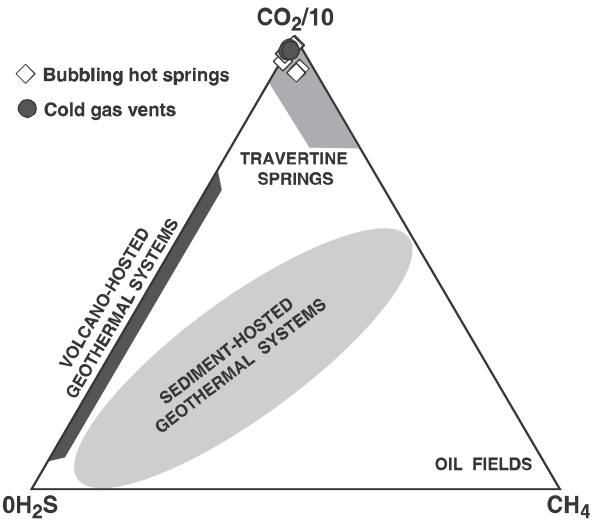

Fig. 5. Ternary plot of CH_4–CO_2–H_2S after Goff et al. (2000) showing fields for volcano-hosted geothermal systems, sediment-hosted geothermal systems, oil field gases, and travertine spring gases. The RVP gases are CO_2-rich and plot in the travertine spring field consistent with extensive travertine deposits in the region.

distillation process cannot easily account for an order of magnitude elemental fractionation between N_2 and He, except perhaps for extreme degrees of open system (Rayleigh) distillation. Nitrogen from thermal decomposition of biogenic material, or biologically mediated processes such as denitrification (N_2 gas production from nitrate) or nitrification (nitrate production from ammonia) can have a wide range of $\delta^{15}N$ values in the range of −20‰ to +20‰ (Sharp, 2007).

In contrast to the wide range in isotope compositions expected from bacterial mediated processes such as nitrification and denitrification the gas samples from RVP display a restricted range in $\delta^{15}N$ between −5.9‰ and +2.0‰, which is generally consistent with source controls on nitrogen isotope compositions (i.e. mixing between mantle, sedimentary, and atmospheric N_2). Considering the large isotopic fraction effects associated with nitrification (nitrate production) and denitrification (N_2 gas production), it is unlikely that these processes play a fundamental control on the nitrogen isotope and N_2/He systematics of the RVP gases because a much larger range in the N isotope compositions would be expected. Nevertheless, the samples that fall significantly outside of the three-component mixing model in Fig. 8 may have been affected by a relatively small amount of N_2 addition if the $\delta^{15}N$ of the bacterially or thermally produced N_2 was <−5‰. Further assessment of fractionation between ammonia, nitrate, and N_2 gas and bacterial nitrification/denitrification as well as thermal decomposition of biogenic sources in geothermal systems would be a productive avenue for future research in gas geochemistry, but is beyond the scope of this study.

Three sampling localities show evidence of N_2 contribution from sedimentary sources: Mampulo and Kasimulo springs in the south, and Ikama Village bubbling stream in the central zone. Ikama Village bubbling stream (EAR6) has a $\delta^{15}N$ value of +2.0‰, N_2/He of 2980, and N_2/O_2 of 10.3. This sample was taken from a swampy area in the central zone (Fig. 1) in shallow water with vegetation where gas was bubbling through sediments. Mampulo spring 2 (EAR4) has a $\delta^{15}N$ value of −0.9‰, with N_2/He of 107, and N_2/O_2 of 16.4. The second sample from Mampulo spring 2 (EAR15) has a $\delta^{15}N$ value of −2.9‰ with N_2/He of 135 and N_2/O_2 of 3.8. Mampulo spring 2 and Kasimulo spring are located in the south of RVP where ancestral Lake Malawi sediments are prominent (Fig. 1). Modern Lake Malawi sediments have $\delta^{15}N$ compositions of ~+3‰ (Filippi and Talbot, 2005), similar to the $\delta^{15}N$ value of the sample from Ikama Village bubbling stream. All four of these samples plot close to the mixing line between mantle and sediment endmembers in Fig. 8 and EAR6 (Ikama Village) and EAR4 (Mampulo spring 2) also have higher than air N_2/O_2 ratios (Fig. 9). We suggest that the sedimentary signature, identified strongly only in one sample, from Ikama Village bubbling stream, is probably a near-surface addition of N_2 from the local sedimentary environment because sample localities nearby (e.g. Ikama Village cold fumarole; EAR5) have some of the strongest mantle signatures in the region. The high N_2/O_2 ratio of the Ikama Village bubbling stream sample is likely due to addition of N_2 from a shallow sedimentary source, consistent with the high N_2/He ratio. The high N_2/O_2 ratio of the one Mampulo spring 2 sample (EAR4) is likely the result of O_2 consumption due to near surface oxidation processes, consistent with the high total S content of this sample and mantle N_2/He and N_2/Ar ratios. Fig. 9 shows no correlation between N_2/O_2 and $\delta^{15}N$ indicating that O_2 addition or removal in the spring systems is independent of the processes that control the nitrogen isotope composition.

The location of hydrothermal features in the RVP is controlled by faults (Fig. 1), which probably also control the hydrology of the deep and shallow aquifers. Delalande et al. (2011) showed that the shallow, cold aquifer is dominated by meteoric water which is underlain by a hot (>110 °C) deep and saline hydrothermal system. Application of the H_2–Ar gas geothermometer of Giggenbach (1991) results in calculated equilibration temperatures of 62 ± 17 °C (Table 2). These temperatures probably reflect gas equilibration with moderate-temperature fluids similar to the highest temperature springs observed in the RVP geothermal system at the lower elevation sites in the north and south.

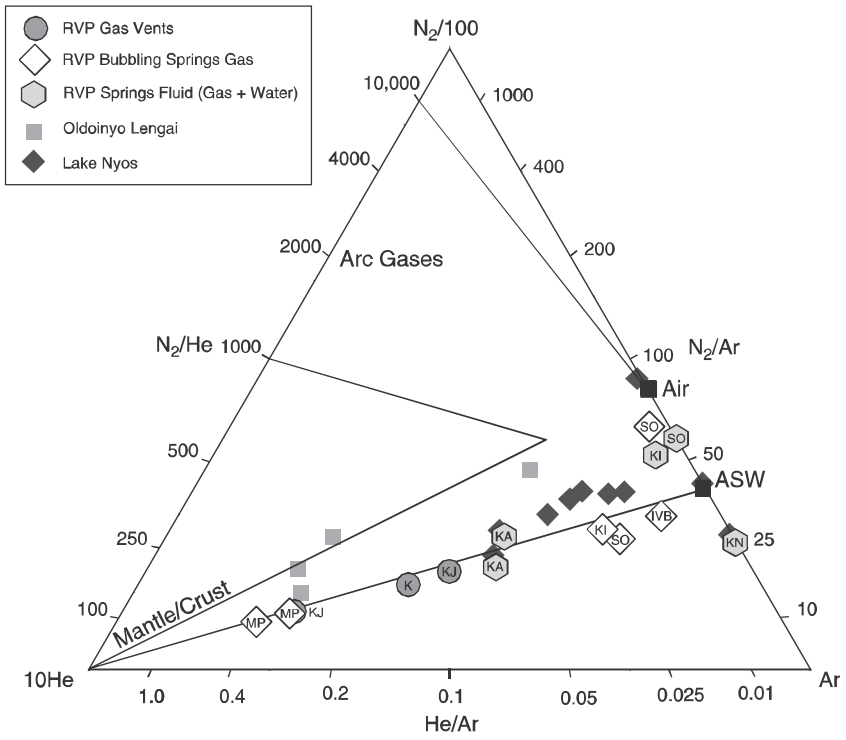

Fig. 6. Ternary plot of N_2–He–Ar with endmember fields for mantle/crustal gases, arc-related gases, as well as the values for air and air saturated water (ASW). The RVP samples plot on a well-defined trend between ASW and the mantle/crustal He apex. Helium may be derived from mantle sources or from decay of radiogenic elements in the crust, however He isotope compositions display an unambiguous upper mantle signature (Pik et al., 2006; Barry et al., 2013–this issue). Compositions of gases from Oldoinyo Lengai (northern Tanzania; Fischer et al., 2009) and Lake Nyos (Cameroon; Giggenbach, 1990) are shown for comparison. SO = Songwe, MP = Mampulo, KI = Kilambo, KA = Kasimulo, KN = Kafwira Njuni, IVB = Ikama Village bubbling stream, K = Kibila cold vent, KJ = Kiejo cold vent.

The CO_2–Ar geothermometer of Giggenbach (1991) suggests much higher temperatures of 279 ± 8 °C (Table 2) and the CO_2–CH_4 gas geothermometer of Taran (1986) results in maximum temperatures of 255 ± 59 °C. These calculated temperatures perhaps represent gas equilibration (CO_2–Ar and CO_2–CH_4 equilibrate slowly relative to H_2–Ar; Giggenbach, 1991) with hotter hydrothermal fluids deeper in the system. The observation that H_2/Ar, CO_2/Ar and CO_2–CH_4 geothermometry results in disparate temperatures is interpreted to reflect a process whereby volatiles originate from the deep higher temperature hydrothermal zone and migrate into the shallow aquifers where they re-equilibrate to lower temperatures before discharging at the surface. The cold gas vents with temperatures of 13–15 °C are found at higher elevations, closer to the recharge zones (Rungwe is 3000 m in elevation) where cold meteoric water infiltrates the hydrothermal system. Higher temperature springs are located in the low-lying areas in the north and south where hot liquids are not as affected by cold recharge. Based on stable isotope compositions of spring discharges, Delalande et al. (2011) concluded that meteoric recharge as sampled by the springs occurred at high elevation or during colder than present climactic conditions. Degassing of dominantly mantle-derived volatiles exsolved from the cold aquifer recharged at the higher elevation central zone, possibly in conjunction with adiabatic expansion and cooling during release to the surface, is the most reasonable explanation for the below ambient temperature of the mantle gases emitted at the cold gas vents (also see Barry et al., 2013–this issue).

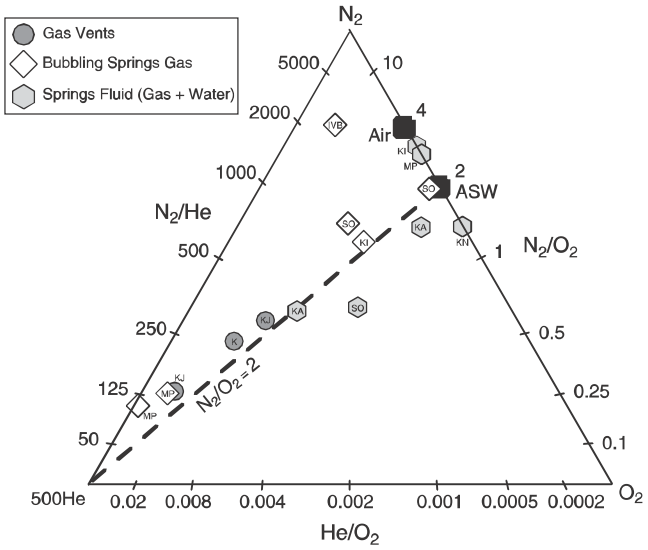

Fig. 7. Ternary plot of N_2–He–O_2. All of the RVP gases have N_2/O_2 ratios similar to ASW and extend towards the He apex, yet nitrogen isotope compositions are clearly distinct from air (Fig. 3). SO = Songwe, MP = Mampulo, KI = Kilambo, KA = Kasimulo, KN = Kafwira Njuni, IVB = Ikama Village bubbling stream, K = Kibila cold vent, KJ = Kiejo cold vent.

5.2. Deep sources

Ratios of chemically non-reactive gas species such as He, Ar, and N_2, as well as isotope compositions, can be used as tracers for volatile source characteristics. Fig. 6 shows a well-defined mixing trend between gases with high He/Ar and low N_2/He and gases with low He/Ar and high N_2/He, which is consistent with mixing between He-rich mantle gases and air saturated water (ASW) or air. Barry et al. (2013–this issue) show that only three sample localities (Kibila cold vent, Ikama Village bubbling stream, and the Kiejo cold vent) have upper mantle or SCLM $^3He/^4He$ ratios of 6–7 R_A and the rest of the hydrothermal system is characterized by relatively low $^3He/^4He$ values (1 to 5 R_A) as the result of mixing between mantle-derived volatiles and ^4He produced by radioactive decay of U- and Th-series radionuclides in the crust. This crustal contribution reduces the initial $^3He/^4He$ ratios from sub-continental

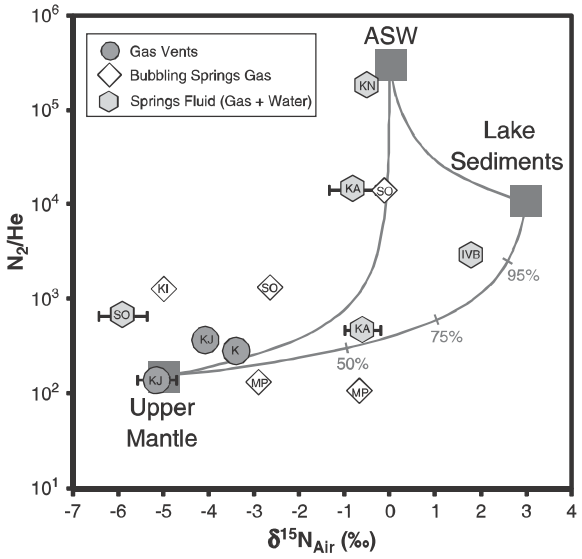

Fig. 8. Plot of N_2/He versus $\delta^{15}N_{Air}$ values with endmembers for upper mantle (Marty and Zimmermann, 1999), ASW, and Lake Malawi sediments (Filippi and Talbot, 2005), after Fischer et al. (2002). Mixing lines between endmembers are also shown. The samples with N_2/He ratios most similar to upper mantle also have nitrogen isotope compositions in the mantle range. The mantle-like samples are from the cold gas vents, which also have He isotope compositions similar to upper mantle (Pik et al., 2006; Barry et al., 2013–this issue). SO = Songwe, MP = Mampulo, KI = Kilambo, KA = Kasimulo, KN = Kafwira Njuni, IVB = Ikama Village bubbling stream, K = Kibila cold vent, KJ = Kiejo cold vent.

lithospheric (SCLM) mantle values (Barry et al., 2013–this issue). Gases with strong crustal He contribution could therefore be expected to have high He/Ar and low N_2/He, though addition of crustal volatiles may also contribute Ar and N_2 as is exemplified by the sample with positive $\delta^{15}N$. The RVP is located in a rift basin with deep crustal thickness (~42 km; Camelbeeck and Iranga, 1996) set in Precambrian basement rocks (dominantly the Proterozoic Ubendian gneiss, which overlies Archean cratonic granites; Begg et al., 2009). The age and composition of this thick crust therefore make for a potentially significant source of ^{4}He and other crustal volatiles, and may contribute to the high He content of RVP gases.

Fig. 10 shows that the majority of samples have CO_2/N_2 ratios within the upper mantle value of 85–190 (Marty and Zimmermann, 1999). Three samples, one from Ikama Village bubbling stream and two water samples (one from Kafwira Njuni and one from Songwe spring) have CO_2/N_2 values below the mantle endmember. These samples have experienced shallow level sedimentary nitrogen addition in the case of Ikama Village bubbling stream, and/or removal of CO_2 due to calcite precipitation, in the case of Kafwira Njuni and Songwe springs (also see Barry et al., 2013–this issue). Of the samples that plot within the mantle CO_2/N_2 ratio field, those collected from the cold CO_2 vents plot closest to the gases from Oldoinyo Lengai Volcano (from Fischer et al., 2009), which are considered the most pristine representation of upper or SCL mantle in the region. These samples also have $\delta^{15}N$ values ranging from −3.4 to −5.2‰, consistent with an upper mantle signature as observed in Oldoinyo Lengai gases (Fig. 8). We consider these samples to be most representative of the nitrogen isotope composition of the mantle source below RVP. In Fig. 10 the majority of the RVP samples scatter around a linear array between a low N_2/He component (Mampulo springs: "MP" in Fig. 10) and a high N_2/He component (Songwe springs: "SO" in Fig. 10) at relatively constant CO_2/N_2 (the average of the samples, excluding the three low CO_2/N_2 samples discussed above, is 160 ± 63, i.e. within the CO_2/N_2 range for mantle). Secondary processes affecting CO_2 and N_2 concentrations can be ruled out as the primary cause of the variable N_2/He and CO_2/He observed in the samples with relatively constant CO_2/N_2 because: 1) liquid–vapor phase separation would cause CO_2 and N_2 to fractionate due to their vastly different solubilities in water (Ellis and Golding, 1963; Weiss, 1971; Taran, 2005), 2) calcite precipitation would not affect N_2 and would therefore result in lower than mantle CO_2/N_2 ratios and 3) shallow CO_2 contribution from crustal limestone alone would result in an increase of the CO_2/N_2 ratio. This last process cannot be completely ruled out in the case of Songwe spring gas samples, due to their slightly higher than mantle CO_2/N_2 ratios. Based on these constraints, the most plausible process to explain the observed variations in CO_2/He and N_2/He ratios at constant CO_2/N_2 are variations in the amount of He ([He]), which drives variability in N_2/He and CO_2/He but does not affect CO_2/N_2. Fig. 11a and b shows that samples with low CO_2/He and N_2/He ratios have high [He], as represented by Mampulo springs in the south. Mampulo springs also have the highest calculated crustal He contribution (Barry et al., 2013–this issue) and fall close to the mantle–sediment mixing line in Fig. 8, indicating that these springs have the greatest crustal volatile contribution in the RVP. The observation that these samples fall below the mantle–sediment mixing is attributed to crustal He contribution from both old basement rocks and shallow sedimentary N_2 addition. The cold CO_2 gas vents plot at intermediate He contents and have mantle-like CO_2/He, N_2/He and He/Ar ratios and $\delta^{15}N$ signatures. Helium isotope compositions also show that the cold gas vents carry the most pristine mantle (SCLM) signature (Pik et al., 2006; Barry et al., 2013–this issue). These vents occur within the Bouger gravity low (Fig. 1) interpreted to reflect the presence of magmatic material at shallow crustal depths by Ebinger et al. (1989) and close to the most recently active volcanoes in the region (Kiejo and Rungwe). Samples with high CO_2/He and N_2/He ratios have low helium concentrations, best represented by Songwe springs in the north. Gas and water samples from Songwe also exemplify the samples that fall well outside of the mixing polygon in Fig. 8, perhaps indicating N_2 addition and/or isotopic fractionation processes (Section 5.1) associated with biological activity or thermal degradation of biogenic sources. The Songwe springs gases also have the highest organic carbon contribution (Barry et al., 2013–this issue), consistent with this interpretation.

In summary, gases collected from the center of Bouger gravity low (i.e. the cold vents) have strong and consistent mantle signatures ($\delta^{15}N$, N_2/He, He/Ar, CO_2/N_2, this study; ^{3}He/^{4}He, $\delta^{13}C$, and $CO_2/^3$He; Barry et al., 2013–this issue). Samples collected from locations outside of the Bouger gravity low (Mampulo, Kasimulo, and Songwe springs, Fig. 1; Ebinger et al., 1989) have highly variable He contents, N isotope compositions, and tracer gas ratios. At Mampulo springs in the south, He

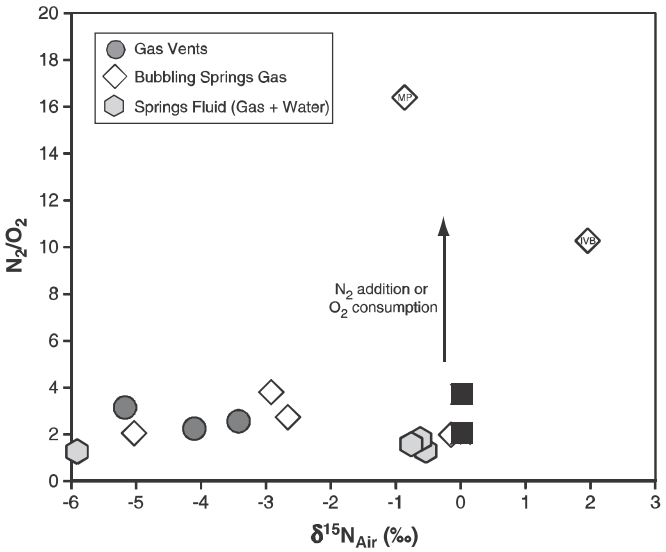

Fig. 9. N_2/O_2 versus $\delta^{15}N_{Air}$. The lack of correlation between nitrogen isotope compositions and N_2/O_2 suggests that the processes of O_2 addition are independent of N_2 source. MP = Mampulo, IVB = Ikama Village bubbling stream.

Table 2
Results of gas geothermometry calculations for gas samples from RVP. All temperatures are reported in °C.

Sample location	ID	log (XH_2/XAr)	T (H_2–Ar)[a]	log (XCO_2/XAr)	T (CO_2/Ar)[a]	log (CO_2/CH_4)	T (CO_2–CH_4)[b]
Songwe spring mesa	EAR1	−1.81	48.6	3.87	280	4.86	204
Songwe spring quarry	EAR17	−1.47	72.0	4.10	290	5.68	174
Kibila cold vent	EAR5	−1.66	58.7	3.78	276	3.60	273
Kiejo cold vent	EAR3	−2.06	30.5	3.74	274	4.03	246
Kiejo cold vent	EAR10	−1.31	83.3	4.10	291	3.92	252
Kilambo springs	EAR19	−1.72	54.3	3.69	271	4.58	217
Mampulo spring 2	EAR4	−1.45	73.4	3.79	276	2.82	335
Mampulo spring 2	EAR15	−1.44	74.4	3.67	270	2.81	337
Average		−1.62	61.9	3.84	279	4.04	255

[a] Giggenbach (1991).
[b] Taran (1986).

isotopes indicate a strong crustal contribution (Barry et al., 2013–this issue), and N_2/He–$\delta^{15}N$ systematics indicate that these gases also contain a significant contribution from crustal (sedimentary) N_2. Kasimulo spring (also located in the south) has strong sedimentary N_2 contribution as well (Fig. 8), and both of these localities occur where ancient Lake Malawi sediments are prevalent (Fig. 1). The hydrothermal discharges in the far north of RVP (Songwe springs) represent samples that have the strongest suggestion of elemental and/or isotopic fractionation, perhaps coupled with biogenic volatile contribution. These samples have the lowest He contents, elevated N_2/He ratios (i.e. outside of mixing polygon in Fig. 8), and high CO_2/He.

We interpret the observation that the gases with the most pristine mantle signatures ($\delta^{15}N$, N_2/He, He/Ar, CO_2/N_2, this study; $^3He/^4He$, $\delta^{13}C$, and $CO_2/_3He$, Barry et al., 2013–this issue) occur close to the intersection of the three structural basins to reflect structural control on mantle volatile migration. These mantle gas emissions also occur near the center of the Bouger gravity anomaly and in the vicinity of structurally controlled voluminous magma extrusion (i.e. alignment of large volcanic edifices of Ngozi, Rungwe, and Kiejo; Fig. 1), indicating that deep crustal structures (fault zones) act as conduits for both mantle volatiles and melts. The relatively high flux of mantle volatiles in the central zone allows the mantle signatures to be maintained. Effects of secondary processes such as crustal volatile contribution and elemental and/or isotopic fractionation are observed at the springs in the northern and southern extremities of the RVP. In the south, samples tend to show N_2/He–$\delta^{15}N$ systematics consistent with sedimentary N_2 addition, and high He concentrations and low $^3He/^4He$ ratios (Barry et al., 2013–this issue) consistent with crustal He contribution. The volatile chemistry of the distal northern springs (Songwe) display more complex or poorly constrained secondary processes, indicated by high N_2/He and CO_2/He ratios and N isotope systematics that may reflect N additional or modification by biogenic sources and He loss during fluid migration.

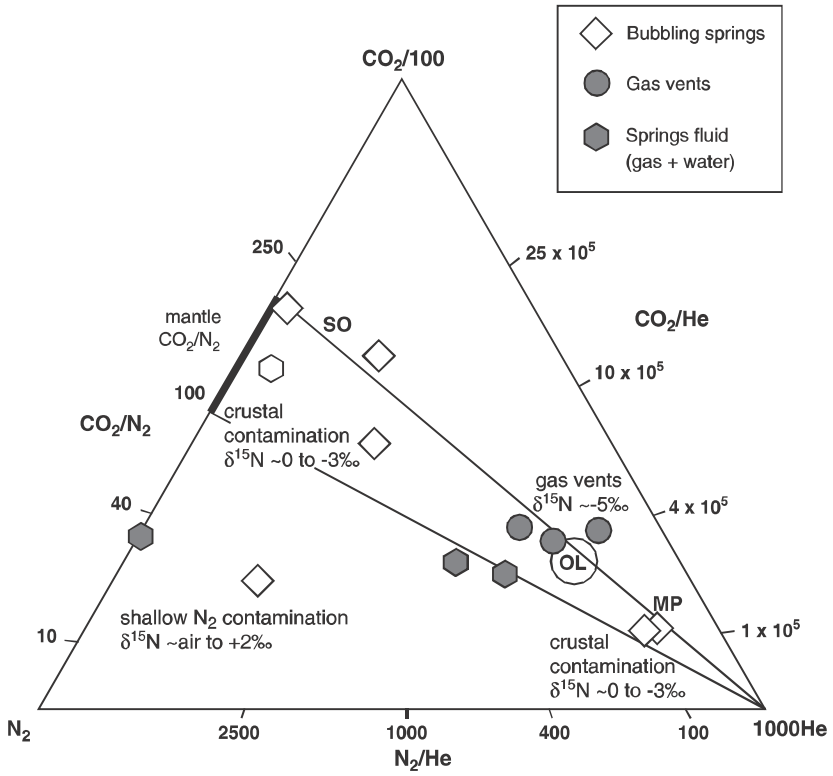

Fig. 10. Ternary plot of CO_2–N_2–He showing the composition of RVP gases and mantle-derived gases from Oldoinyo Lengai (OL) Volcano (Fischer et al., 2009). The majority of samples fall within the mantle CO_2/N_2 range of 80–190 based on MORB glasses (Marty and Zimmermann, 1999). MP is Mampulo springs and SO is Songwe springs. Shallow level N_2 contamination results in lower than mantle CO_2/N_2. Samples from cold gas vents plot close to OL gases representing the RVP mantle abundance ratios. Deviations from the mantle composition are the result of variations in He content of the gases due to crustal contamination with radiogenic He.

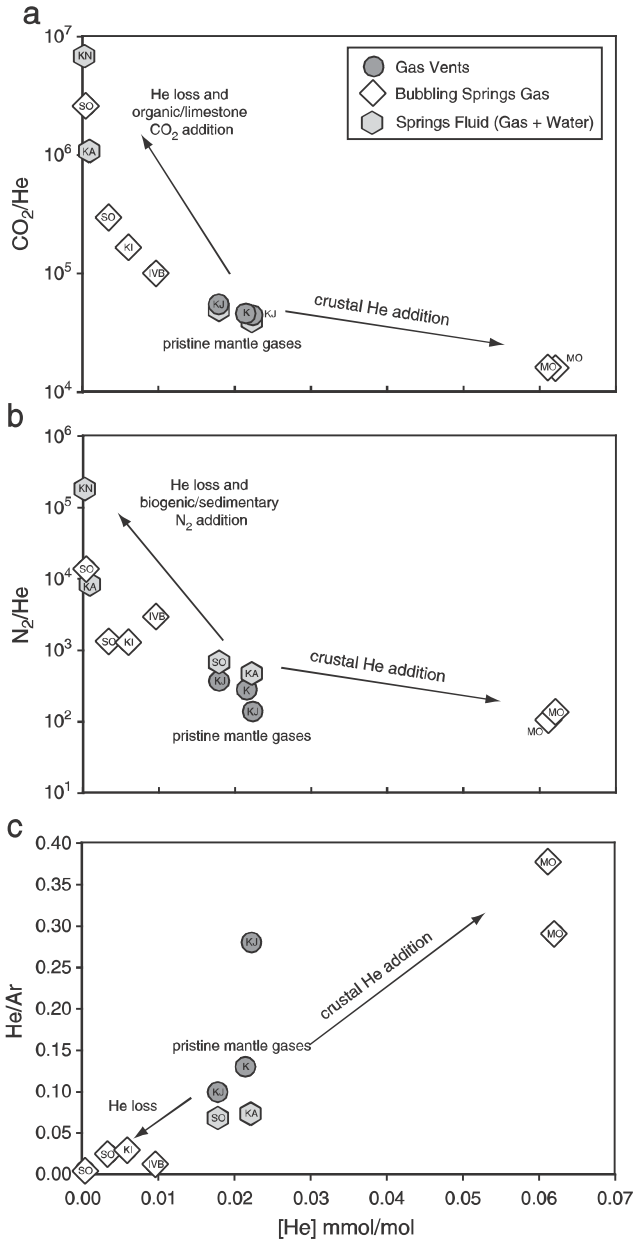

Fig. 11. Three diagrams showing the variation in key gas ratios (CO_2/He, N_2/He and He/Ar) with absolute He content [He] of the samples. All observed ratio variations are predominantly a function of [He]. SO = Songwe, MP = Mampulo, KI = Kilambo, KA = Kasimulo, KN = Kafwira Njuni, IVB = Ikama Village bubbling stream, K = Kibila cold vent, KJ = Kiejo cold vent.

Geothermal activity at Songwe springs may be driven by a magmatic volatile and heat source at Ngozi Volcano, located ~40 km to the southwest of the springs (Kraml et al., 2010). The distance and time involved in this long lateral fluid flow allow sufficient opportunity for multiple shallow processes (such as crustal contribution, fluid degassing, air contamination, and/or bacterial modification) to modify gas compositions from pristine mantle compositions.

5.3. Model of the Rungwe Volcanic Province hydrothermal system

We envision a scenario in which deep hot (~250 °C) saline crustal fluids receive continuous input of ultimately mantle-derived volatiles (CO_2, He and N_2) with variable contribution from crustal-derived volatiles, as described above. Deep geothermal fluids migrate along fault conduits and degas into the shallow, neutral pH and low temperature aquifer (Delalande et al., 2011) and are modified by contributions from air and shallow sedimentary volatiles, the extent of which is determined by local geology and hydrology. The most vigorous degassing and most pristine mantle signatures are observed in the central area, near the intersection of the three structural basins, which is also the focus of magmatic activity and the location of the most direct structural conduit to the mantle. Thus, structural conduits extending through the crust drive mountain building through magmatism and also provide mantle-derived volatiles access to the surface. The observation that the degassing phenomena in the central region are low temperature is attributed to two related processes 1) gases released from the low-temperature (~62 °C), shallow level aquifer are further cooled by interaction with high elevation meteoric recharge. This process is evident at Ikama bubbling stream, located nearby the gas vents where gases discharge through a stream of 23 °C; and 2) gases released from the liquid phase are further cooled by migrating through water saturated strata to the surface. The shallow infiltrating cold meteoric waters do not introduce significant atmospheric CO_2, N_2, or radiogenic He (based on isotopic compositions of the gases and the arguments presented above in Sections 5.1 and 5.2) because they are too young to dissolve significant amounts of these gases to affect abundance or isotopic ratios. The gas content of the shallow aquifer is dominated by mantle-derived CO_2, N_2, and He which also dominate the gas compositions sampled at the surface.

A schematic cross section of the Rungwe area is shown in Fig. 12. Volatiles and heat from the SCLM enter the saline aquifer along deep rift faults. As volatiles enter at depth, gases are released from the deep hydrothermal zone into the shallow aquifer along faults located in the central portion of the rift consistent with the location of the recent volcanics and springs. Meteoric water and atmospheric gases enter the shallow aquifer and mix with deep volatiles. The flux of deep CO_2 into the shallow aquifer dominates the overall volatile budget. The CO_2 factory at Kiejo collects approximately 1.6×10^5 mol CO_2 per year (~800 g CO_2/h, as routinely measured at the plant during normal operation). Using the CO_2/N_2 ratio of the Kiejo gas samples and assuming that all N_2 at this site is mantle derived ($\delta^{15}N = -4.6‰$) we calculate that the mantle-derived N_2 flux is 6.8×10^2 mol/year. Currently, there are no estimates of volatile fluxes for the East African Rift system as a whole and this topic should receive high priority in future studies in order to better constrain global volatile transfer from the mantle to the Earth's surface at continental rifts.

6. Conclusions

We report here the first complete gas chemistry and nitrogen isotope compositions of cold CO_2 vents and spring discharges in the Rungwe region and one of the first in the entire East African Rift. The region is characterized by extensional faulting and structurally controlled volcanism. Springs and vigorously discharging cold CO_2 vents are mostly located along major faults, which are efficient structural conduits of mantle-derived volatiles to the surface. Our data show that shallow-level processes (crustal contamination and atmospheric contamination are the most clearly identified) have modified the compositions of a number of samples, particularly those from springs located in the distal northern and southern RVP. Relatively pristine mantle-derived gases (in terms of CO_2–N_2–Ar–He systematics and nitrogen isotope compositions) are emitted at vigorous cold gas vents in the central, higher elevation RVP area indicating that the focus of mantle-derived volatile degassing is associated with the intersection of the three structural basins and the center of a Bouger gravity anomaly, which is interpreted to reflect structural control on both mantle degassing and magmatic activity. Application of gas geothermometers shows a wide range in equilibrium temperatures from ~70 °C to >250 °C, which are consistent with but more variable than previous geothermometric estimations. The highest equilibrium temperatures may represent conditions in a deep saline

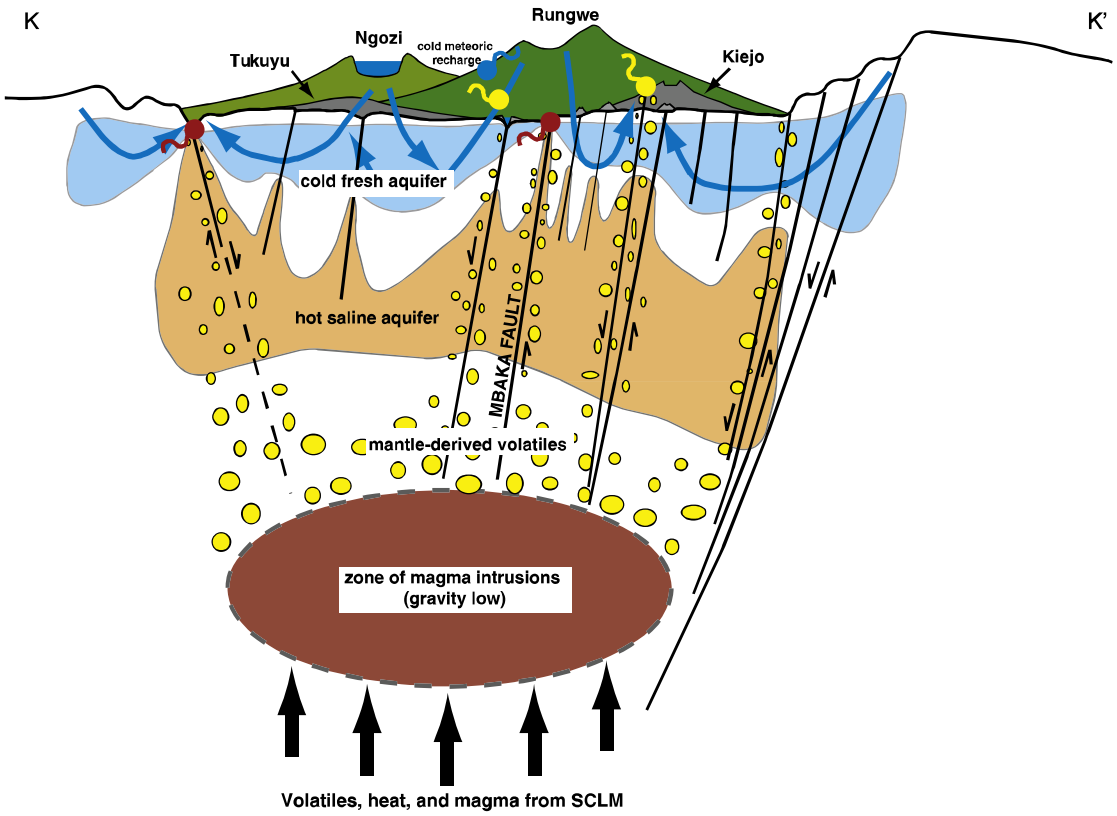

Fig. 12. Schematic cross section of the RVP geothermal system along the K–K′ transect from Ebinger et al. (1989) shown in Fig. 1. Structural interpretation is taken directly from Ebinger et al. (1989). Volcanic edifices located to the north of the cross section line are projected onto the section. Mantle-derived volatiles are channeled to the surface by fault conduits. Cold meteoric recharge from the volcanic highlands creates a cold, fresh water lens resulting in low temperature gas emissions at the higher elevation springs and vents. Hot springs occur on the edges of the hydrothermal system in lower elevation areas far from the meteoric recharge zone in the volcanic highlands.

fluid, whereas the regionally consistent temperatures of ~70 °C derived from the H_2–Ar geothermometer (Giggenbach, 1990) suggest that the RVP gases last equilibrated with a shallow, relatively low temperature geothermal reservoir. Naturally-occurring cold (13 °C) vents are features where CO_2-dominated gases discharge through fissures. Our data show that mantle volatile discharges are prolific in this section of the rift and that further study is needed to characterize the overall extent of mantle degassing for hazard assessment and evaluation of the geothermal potential of the region. Further work is also needed to determine the gas fluxes from the entire East African Rift in order to constrain this potentially significant pathway of mantle volatiles to the Earth's surface.

Acknowledgments

We thank Cindy Ebinger for providing topographic maps of the Rungwe region which were important for locating access to the springs and CO_2 vents. The staff of the Kiejo CO_2 factory is acknowledged for their logistical support during fieldwork at the CO_2 vents and for a tour of the facility. Dennis Newell is acknowledged for early developments of the nitrogen isotope technique that led to the method presented here. We thank Ryan Crow for assistance with ArcGIS. The US National Science Foundation (NSF), Earth Science Division, is acknowledged for funding through grant # 0827352 for field work and EAR/IF grant # 0743540, both to TPF. Fieldwork was also supported by discretionary funds from the Fluids and Volatiles Laboratory, Scripps Inst. Oceanography. A NASA Earth and Space Science Fellowship (NESSF) supported JMdM during this work and the manuscript was completed during an NSF IPA appointment to TPF.

References

Ambraseys, N.N., 1991. The Rukwa Earthquake of 13 December 1910 in East-Africa. Terra Nova 3 (2), 202–211.
Barry, P.H., et al., 2013. Helium and carbon isotope systematics of cold "mazuku" CO_2 vents and hydrothermal gases and fluids from Rungwe Volcanic Province, southern Tanzania. Chemical Geology 339, 141–156 (this issue).
Begg, G.C., et al., 2009. The lithospheric architecture of Africa: seismic tomography, mantle petrology, and tectonic evolution. Geosphere 5 (1), 23–50.
Biggs, J., Nissen, E., Craig, T., Jackson, J., Robinson, D.P., 2010. Breaking up the hanging wall of a rift-border fault: the 2009 Karonga earthquakes, Malawi. Geophysical Research Letters 37.
Boyd, S.R., Pillinger, C.T., Milledge, H.J., Mendelssohn, M.J., Seal, M., 1992. C-isotopic and N-isotopic composition and the infrared-absorption spectra of coated diamonds — evidence for the regional uniformity of CO_2–H_2O rich fluids in lithospheric mantle. Earth and Planetary Science Letters 109 (3–4), 633–644.
Burnard, P., Graham, D., Turner, G., 1997. Vesicle-specific noble gas analyses of "popping rock": implications for primordial noble gases in earth. Science 276 (5312), 568–571.
Camelbeeck, T., Iranga, M.D., 1996. Deep crustal earthquakes and active faults along the Rukwa trough, Eastern Africa. Geophysical Journal International 124 (2), 612–630.
Cartigny, P., 2005. Stable isotopes and the origin of diamond. Elements 1 (2), 79–84.
Chiodini, G., 1994. Temperature, pressure and redox conditions governing the composition of the cold CO_2 gases discharged in north Latium (Central Italy). Applied Geochemistry 9 (3), 287–295.
Crossey, L.J., et al., 2009. Degassing of mantle-derived CO(2) and He from springs in the southern Colorado Plateau region—neotectonic connections and implications for groundwater systems. Geological Society of America Bulletin 121 (7–8), 1034–1053.
de Moor, J.M. et al., submitted for publication. Extremely volatile-rich silicate melts from Oldoinyo Lengai Volcano (Tanzania): implications for carbonatite genesis and eruptive behavior. Earth and Planetary Science Letters.
Delalande, M., Bergonzini, L., Branchu, P., Filly, A., Williamson, D., 2008. Hydroclimatic and geothermal controls on the salinity of Mbaka Lakes (SW Tanzania): limnological and paleolimnological implications. Journal of Hydrology 359 (3–4), 274–286.
Delalande, M., et al., 2011. Fluid geochemistry of natural manifestations from the Southern Poroto-Rungwe hydrothermal system (Tanzania): preliminary conceptual model. Journal of Volcanology and Geothermal Research 199 (1–2), 127–141.
Ebinger, C.J., Deino, A.L., Drake, R.E., Tesha, A.L., 1989. Chronology of volcanism and rift basin propagation — Rungwe Volcanic Province, East-Africa. Journal of Geophysical Research-Solid Earth and Planets 94 (B11) (15785-&).

Elkins, L.J., et al., 2006. Tracing nitrogen in volcanic and geothermal volatiles from the Nicaraguan volcanic front. Geochimica Et Cosmochimica Acta 70 (20), 5215–5235.
Ellis, A.J., Golding, R.M., 1963. The solubility of carbon dioxide above 100 °C in water and sodium chloride solutions. American Journal of Science 261, 47–60.
Filippi, M.L., Talbot, M.R., 2005. The palaeolimnology of northern Lake Malawi over the last 25 ka based upon the elemental and stable isotopic composition of sedimentary organic matter. Quaternary Science Reviews 24 (10–11), 1303–1328.
Fischer, T.P., Giggenbach, W.F., Sano, Y., Williams, S.N., 1998. Fluxes and sources of volatiles discharged from Kudryavy, a subduction zone volcano, Kurile Islands. Earth and Planetary Science Letters 160 (1–2), 81–96.
Fischer, T.P., et al., 2002. Subduction and recycling of nitrogen along the central American margin. Science 297 (5584), 1154–1157.
Fischer, T.P., et al., 2009. Upper-mantle volatile chemistry at Oldoinyo Lengai Volcano and the origin of carbonatites. Nature 459 (7243), 77–80.
Fontijn, K., et al., 2010. Holocene explosive eruptions in the Rungwe Volcanic Province, Tanzania. Journal of Volcanology and Geothermal Research 196 (1–2), 91–110.
Furman, T., 1995. Melting of metasomatized subcontinental lithosphere - undersaturated mafic lavas from Rungwe, Tanzania. Contributions to Mineralogy and Petrology 122 (1-2), 97–115.
Giggenbach, W.F., 1988. Geothermal solute equilibria — derivation of Na–K–Mg–Ca geoindicators. Geochimica Et Cosmochimica Acta 52 (12), 2749–2765.
Giggenbach, W.F., 1990. Water and gas chemistry of Lake Nyos and its bearing on the eruptive process. Journal of Volcanology and Geothermal Research 42 (4), 337–362.
Giggenbach, W.F., 1991. Chemical Techniques in Geothermal Exploration. UNITAR.
Giggenbach, W.F., Goguel, R.L., 1989. Methods for the Collection and Analysis of Geothermal and Volcanic Water and Gas Samples, Rep. CD 2387. Chem. Div., Dept. of Sci. and Ind. Res., Petone, N. Z., p. 53.
Goff, F., et al., 2000. Contrasting hydrothermal activity at Sierra Negra and Alcedo Volcanoes, Galapagos Archipelago, Ecuador. Bulletin of Volcanology 62 (1), 34–52.
Harkin, D.A., 1960. The Rungwe volcanics at the northern end of Lake Nyasa. Memoir II. Geological Survey of Tanganyika, Dodoma. 172 pp.
Hilton, D.R., et al., 2011. Helium isotopes at Rungwe Volcanic Province, Tanzania, and the origin of East African Plateaux. Geophysical Research Letters 38.
Inguaggiato, S., Taran, Y., Fridriksson, T., Melian, G., D'Alessandro, W., 2009. Nitrogen isotopes in volcanic fluids of different geodynamic settings. Geochimica et Cosmochimica Acta 73, A569-A569.
Koepenick, K.W., et al., 1996. Volatile emissions from the crater and flank of Oldoinyo Lengai Volcano, Tanzania. Journal of Geophysical Research-Solid Earth 101 (B6), 13819–13830.
Kraml, M., Mnjokava, T.T., Mayalla, J.W., Kabaka, K., 2010. Surface exploration of a viable geothermal resource in Mbeya area, SW Tanzania — part ii: geochemistry. Proceedings World Geothermal Congress 2010, Bali, Indonesia, pp. 25–29.
Kusakabe, M., Ohsumi, T., Aramaki, S., 1989. The Lake Nyos gas disaster — chemical and isotopic evidence in waters and dissolved-gases from 3 Cameroonian crater lakes, Nyos, Monoun and Wum. Journal of Volcanology and Geothermal Research 39 (2–3), 167–185.
Li, L., Bebout, G.E., 2005. Carbon and nitrogen geochemistry of sediments in the Central American convergent margin: insights regarding subduction input fluxes, diagenesis, and paleoproductivity. Journal of Geophysical Research-Solid Earth 110 (B11).
Marty, B., Zimmermann, L., 1999. Volatiles (He, C, N, Ar) in mid-ocean ridge basalts: assessment of shallow-level fractionation and characterization of source composition. Geochimica Et Cosmochimica Acta 63 (21), 3619–3633.
Marty, B., Pik, R., Gezahegn, Y., 1996. Helium isotopic variations in Ethiopian plume lavas: nature of magmatic sources and limit on lower mantle contribution. Earth and Planetary Science Letters 144 (1–2), 223–237.
Mitchell, E.C., et al., 2010. Nitrogen sources and recycling at subduction zones: insights from the Izu–Bonin–Mariana arc. Geochemistry, Geophysics, Geosystems 11 (2).
Nyblade, A.A., Robinson, S.W., 1994. The African superswell. Geophysical Research Letters 21 (9), 765–768.
Palot, M., Cartigny, P., Viljoen, F., 2009. Diamond origin and genesis: A C and N stable isotope study on diamonds from a single eclogitic xenolith (Kaalvallei, South Africa). Lithos 112, 758–766.
Peters, K.E., Sweeney, R.E., Kaplan, I.R., 1978. Correlation of carbon and nitrogen stable isotope ratios in sedimentary organic-matter. Limnology and Oceanography 23 (4), 598–604.
Pik, R., Marty, B., Hilton, D.R., 2006. How many mantle plumes in Africa? The geochemical point of view. Chemical Geology 226 (3–4), 100–114.
Ritsema, J., van Heijst, H.J., Woodhouse, J.H., 1999. Complex shear wave velocity structure imaged beneath Africa and Iceland. Science 286 (5446), 1925–1928.
Sadofsky, S.J., Bebout, G.E., 2004. Nitrogen geochemistry of subducting sediments: new results from the Izu–Bonin–Mariana margin and insights regarding global nitrogen subduction. Geochemistry, Geophysics, Geosystems 5.
Sano, Y., Takahata, N., Nishio, Y., Fischer, T.P., Williams, S.N., 2001. Volcanic flux of nitrogen from the Earth. Chemical Geology 171 (3–4), 263–271.
Sawyer, G.M., Carn, S.A., Tsanev, V.I., Oppenheimer, C., Burton, M., 2008. Investigation into magma degassing at Nyiragongo volcano, Democratic Republic of the Congo. Geochemistry, Geophysics, Geosystems 9.
Scarsi, P., Craig, H., 1996. Helium isotope ratios in Ethiopian rift basalts. Earth and Planetary Science Letters 144, 505–516. http://dx.doi.org/10.1016/S0012-821X(96)00185-9.
Sharp, Z.D., 2007. Principles of Stable Isotope Geochemistry. Pearson Prentice Hall, Upper Saddle River. 344 pp.
Smets, B., et al., 2010. Dry gas vents ("mazuku") in Goma region (North-Kivu, Democratic Republic of Congo): formation and risk assessment. Journal of African Earth Sciences 58 (5), 787–798.
Snyder, G., Poreda, R., Fehn, U., Hunt, A., 2003. Sources of nitrogen and methane in Central American geothermal settings: noble gas and (129)I evidence for crustal and magmatic volatile components. Geochemistry, Geophysics, Geosystems 4.
Taran, Y.A., 1986. Gas geothermometers for hydrothermal systems. Geokhimiya 3, 339–354.
Taran, Y.A., 2005. A method for determination of the gas–water ratio in bubbling springs. Geophysical Research Letters 32 (L23403). http://dx.doi.org/10.1029/2005GL024547.
Taran, Y., et al., 1998. Geochemistry of the volcano-hydrothermal system of El Chichón Volcano, Chiapas, Mexico. Bulletin of Volcanology 59, 436–449.
Tassi, F., et al., 2009. Water and gas chemistry at Lake Kivu (DRC): geochemical evidence of vertical and horizontal heterogeneities in a multibasin structure. Geochemistry, Geophysics, Geosystems 10.
Tedesco, D., et al., 2010. Gas isotopic signatures (He, C, and Ar) in the Lake Kivu region (western branch of the East African rift system): geodynamic and volcanological implications. Journal of Geophysical Research 115, B01205. http://dx.doi.org/10.1029/2008JB006227.
Vaselli, O., et al., 2003. The "evil winds" (mazukus) at Nyiragongo volcano (Democratic Republic of Congo). Acta Vulcanologica 14–15, 123–128.
Weiss, R.F., 1971. Solubility of helium and neon in water and seawater. Journal of Chemical and Engineering Data 16 (2), 235–241.
Zimmer, M.M., et al., 2004. Nitrogen systematics and gas fluxes of subduction zones: insights from Costa Rica arc volatiles. Geochemistry, Geophysics, Geosystems 5.